Fragment Energy and Velocity Measurements in Fission of Uranium by 2.9-GeV Protons*

L. P. Remsberg, F. Plasil,† J. B. Cumming, and M. L. Perlman

Chemistry Department, Brookhaven National Laboratory, Upton, New York 11973

(Received 11 June 1969)

Fission of uranium induced by 2.9-GeV protons was studied with semiconductor detectors and velocity-measuring devices. The angular correlation between members of fission-fragment pairs as well as the energies of the two fragments and the velocities of one were determined. Fragment masses were thus ascertained. From these data, deductions were made about excitation energies and momenta of the fissioning systems. The results show that although there is a much broader mass spectrum of fissioning nuclei produced at 2.9 GeV than is present at lower bombarding energies, the fission mechanisms in the two cases are indistinguishable. Mean fragment velocities are found to be very nearly independent of fissioning-system mass, in agreement with calculations based on a liquid-drop model.

I. INTRODUCTION

FISSION of uranium induced by high-energy protons has been studied for many years by a variety of techniques.[1] Radiochemical and mass-spectrometric cross-section measurements have been used to obtain charge-dispersion curves at individual product masses[2–7]; these curves have been integrated to obtain mass yield distributions, which are broad, symmetric peaks centered at $A \approx 110$.[8] For bombarding energies above ~ 1 GeV, the charge-dispersion curves broaden with increasing mass and become double-peaked for $A \gtrsim 110$.[8] Thick-target, thick-recoil-catcher experiments at these energies have shown that the neutron-deficient products have considerably smaller momenta than do the neutron-excess products.[3,4,9] Both this result and the double-peaked charge-dispersion curves suggest that more mechanisms than one contribute to the formation of products in the fission-mass region at high incident proton energies. Double-differential cross sections $d^2\sigma/d\Omega dR$ measured for selected products at various angles in thin-target, thin-catcher recoil experiments have recently been interpreted to indicate that at 2.2 GeV there is only one general fission mechanism operative, and that there is a small contribution in the fission-mass region from a nonfission spallationlike mechanism.[10]

While radiochemical techniques can yield product charge and mass distributions and even double-differential cross sections for individual products, they cannot provide direct evidence for the presence or absence of a major partner fragment. Dielectric detectors can be used to register track pairs produced by the major fragments in fission; total cross sections for fission, for breakup into three major fragments,[11,12] as well as more detailed information such as track-length ratios and angular correlations, have been obtained with this technique.[13] Little or no information on the energy, mass, or charge of fragments is obtainable, however.

Semiconductor detectors have been employed in the study of low- and medium-energy fission to measure the energies and, by means of conservation laws, the masses of coincident fragments.[14] This technique has been extended to the study of fission induced by 156-MeV protons[15,16]; but, since the momenta of the fissioning nuclei were not known, conservation laws could not be used and only fragment energies and angles could be determined.

In the study of the fission of uranium by 2.9-GeV protons described herein, semiconductor detectors were used, but, in addition to the energies and angles of both members of fragment pairs, the velocity, and hence the

* Research performed under the auspices of the U. S. Atomic Energy Commission.

† Present address: Oak Ridge National Laboratory, Oak Ridge, Tenn. 37830.

[1] For a general summary of high-energy reactions with an emphasis on fission see E. K. Hyde, *The Nuclear Properties of the Heavy Elements* (Prentice-Hall, Inc., Englewood Cliffs, N. J., 1964), Vol. III.

[2] G. Friedlander, L. Friedman, B. Gordon, and L. Yaffe, Phys. Rev. **129**, 1809 (1963).

[3] J. M. Alexander, C. Baltzinger, and M. F. Gazdik, Phys. Rev. **129**, 1826 (1963).

[4] G. Rudstam and G. Sørensen, J. Inorg. Nucl. Chem. **28**, 771 (1966).

[5] E. Hagebø, J. Inorg. Nucl. Chem. **29**, 2515 (1967).

[6] N. T. Porile, Phys. Rev. **148**, 1235 (1966).

[7] S. Kaufman, Phys. Rev **129**, 1866 (1963); and private communication as quoted in Ref. 8.

[8] G. Friedlander, *Physics and Chemistry of Fission* (International Atomic Energy Agency, Vienna, 1965), Vol. II, p. 265.

[9] R. Brandt, *Physics and Chemistry of Fission* (International Atomic Energy Agency, Vienna, 1965), Vol. II, p. 329.

[10] V. P. Crespo. J. B. Cumming, and A. M. Poskanzer, Phys. Rev. **174**, 1455 (1968).

[11] R. Brandt, F. Carbonara, E. Cieslak, M. Dakowski, Ch. Gfeller, H. Piekarz, J. Piekarz, W. Riezler, R. Rinzivillo, E. Sassi, M. Sowinski, and J. Zakrzewski, Nucl. Phys. **A90**, 177 (1967).

[12] J. Hudis and S. Katcoff, Phys. Rev. **180**, 1122 (1969).

[13] M. Debeauvais, R. Stein, J. Ralarosy, and P. Cüer, Nucl. Phys. **A90**, 186 (1967).

[14] See, for example, J. S. Fraser and J. C. D. Milton, Ann. Rev. Nucl. Sci. **16**, 379 (1966).

[15] L. Kowalski, C. Stephan, H. Langevin-Joliot, and P. Radvanyi, Phys. Letters **2**, 356 (1962).

[16] C. J. Stephan and M. L. Perlman, Phys. Rev. **164**, 1528 (1967).

mass, of one of the fragments was obtained.[17] This was accomplished by measuring the time difference between the arrival of the fragments at their two respective detectors, one located as near as possible to the target and the other, on the opposite side, far away. With a correction for the approximate flight time of the fragment going into the near detector, this time interval is the flight time of the fragment going into the far detector, which yields the velocity of that fragment directly. These experiments were carried out with the near detector fixed at 90° to the beam direction and with the far detector at various angles, both in and out of the plane defined by the beam and the center of the near detector. The angular correlation was thus mapped, and the energies of both members of fragment pairs as well as the mass of one were measured for individual events at the various angles. Single-fragment-mass distributions and mass-energy correlations were obtained at these angles, but only the mean values of the total masses of fragment pairs could be obtained.

Crespo *et al.*[10] have measured angular distributions of various products from the fission of uranium by 2.2-GeV protons. For each product, the differential cross section at 90° was found to be approximately equal to its total cross section divided by 4π, regardless of whether the angular distribution is peaked forward or nearly isotropic in the laboratory system. This was also the case for the production of Na^{24} from bismuth[18] and Tb^{149} from gold,[19] which presumably do not represent fission. Thus, the fragments observed at 90° are expected to be an unbiased sample of all products in the fission-mass region.

II. EXPERIMENTAL PROCEDURE

Experiments were performed in a 1-m-diam scattering chamber placed at the focus of an external 2.9-GeV proton beam from the Brookhaven Cosmotron. This beam was transported through a vacuum pipe and focused to an approximately round spot such that $\approx$50% of the beam intensity was contained in a 6-mm-diam circle, as determined by foil activation. A diffuse horizontal tail, which severely affected the background counting rates, was largely eliminated by a 75-cm brass collimator placed where the beam left the Cosmotron and a 60-cm lead collimator located just in front of the scattering chamber. Considerable care was taken to ensure that the collimator near the chamber did not intercept any of the central beam spot. Even so, it was found necessary to provide additional lead shielding inside the chamber to screen the detectors from the upstream edge of the lead collimator, which intercepted the diffuse tail and was thus a source of secondary particles. Immediately beyond the scattering chamber, the protons passed through an ionization chamber beam monitor and also through a thin fluorescent screen, which was viewed by television to monitor the position and shape of the beam spot. The beam was then transported in vacuum several meters downstream. Throughout the course of the experiments the beam intensity varied between 2 and 6×10^{10} protons per pulse with a pulse rate of 1 per 4.5 sec. Each beam pulse was about 200 msec in duration, and there was generally no great variation of intensity within this period. The beam entered and left the chamber, which was evacuated to a pressure of $<10^{-4}$ Torr, through 250-μ Mylar windows; these were changed whenever they showed signs of radiation damage.

The target, located at the center of the chamber, consisted of a 5-mm-diam disk of UF_4 which was vacuum-deposited to a thickness of $\approx$200 μg/cm^2 on a 3×4-in. Formvar backing 60 μg/cm^2 in thickness. It was oriented at an angle of 40° with respect to the beam, and the UF_4 deposit faced the distant detectors.

Silicon surface-barrier fission-fragment detectors[20] with resistivities ranging from 400 to 1000 Ω cm were used throughout these experiments, and care was taken to ensure that they were operated at bias voltages within the charge collection plateau and below the onset of charge multiplication.[21] The near detector at 90° had an active area 5.6 mm in diameter and was located 4.9 cm from the target center. An aluminum collimator with a diameter of 4.4 mm was fastened to the front of this detector in order to eliminate resolution-degrading edge effects.[21] On the opposite side of the chamber, four detectors were located 40 cm from the target so that data at four angles could be obtained simultaneously. These detectors were mounted on a remotely controllable arm which could be rotated about the center of the chamber; each had an active area 27.6 mm in diameter and each was covered with an aluminum collimator with a diameter of 25.4 mm. The target-to-detector distances were measured with an accuracy of $\approx$0.5 mm and the various detector angles were measured with an accuracy of $\approx$0.3°. It is very difficult to calculate the angular-correlation resolution function, but the function is roughly bell-shaped with a full width at half-maximum of $\approx$5°. Two 20-mm-diam detectors were located on the diameter of a 10-cm-radius circle centered on the target. This diameter was at an angle of 60° with the beam direction, and the detector pair, in coincidence, served as a fission monitor having a response proportional to the product of the number of protons passing through the target and the uranium thickness. With the

[17] Experiments similar to those described herein are being done at a proton energy of 12 GeV by investigators at the Argonne National Laboratory.

[18] J. B. Cumming, R. J. Cross, Jr., J. Hudis, and A. M. Poskanzer, Phys. Rev. **134**, B167 (1964).

[19] V. P. Crespo, J. B. Cumming, and J. M. Alexander (unpublished).

[20] Detectors were obtained from Ortec, Inc.

[21] H. W. Schmitt and F. Pleasonton, Nucl. Instr. Methods **40**, 204 (1966).

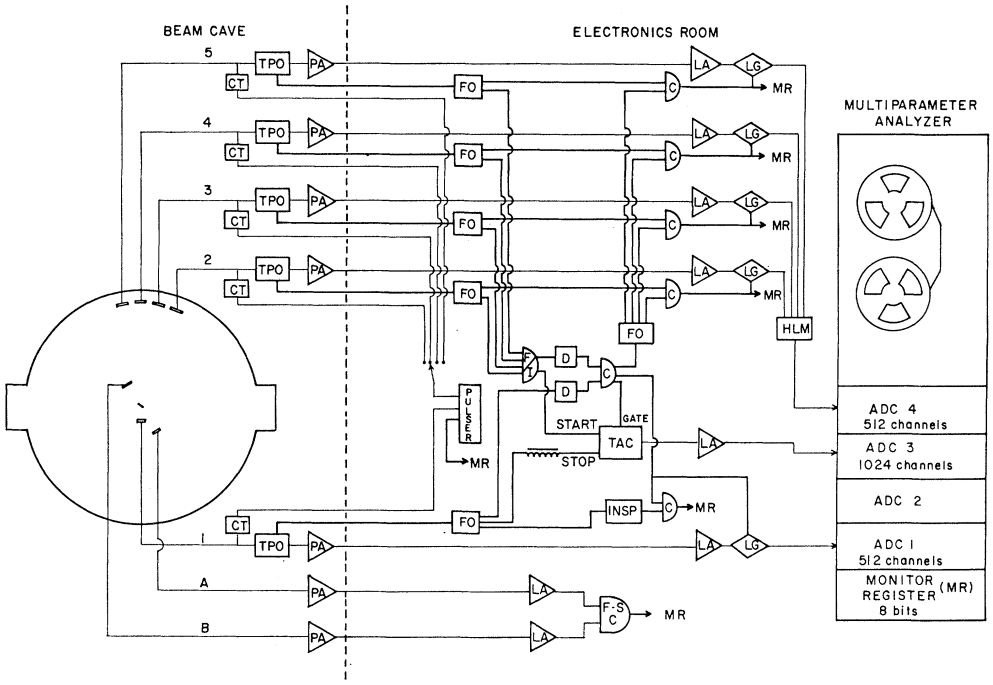

FIG. 1. Schematic diagram of scattering chamber, detectors, and data acquisition system. Meanings of the symbols are as follows: CT, charge terminator; TPO, time pickoff; PA, preamplifier; FO, fan out; FI, fan in; HLM, high-level mixer; ADC, analog-to-digital converter; 1, 2, 3, 4, 5, leads from fission-fragment detectors; A, B, leads from fission monitor detectors; LA, linear amplifier; FSC, fast-slow coincidence; D, discriminator; C, coincidence; TAC, time-to-amplitude converter; and LG, linear gate.

monitor information, data from the various sets of measurements could be normalized.

The electronic equipment consisted of "slow" electronics for processing the pulse-height information from the detectors and "fast" electronics for the time information and also for control logic. A slightly simplified block diagram of this apparatus is shown in Fig. 1. Because of the requirement of a time resolution less than 1 nsec, time information was extracted from pulse-transformer time pickoffs[22] inserted directly between the detectors and the preamplifiers. These devices, which include a variable threshold discriminator, provide nearly jitter-free, leading-edge timing pulses. Time pickoffs, preamplifiers, and charge terminators for insertion of pulser signals were located at the scattering chamber, and the signals were sent to the remainder of the electronics system via 10-m cables. Timing pulses from the four distant detectors were combined so that only one time-to-amplitude converter (TAC) and one coincidence circuit for gating the TAC were necessary. An identification signal indicated which one of the four detectors was associated with the coincidence and also opened only the linear gate associated with that detector. A pulse-pileup inspector, essentially a pulse-pair indicator, was used with the near detector, which had the highest counting rate. Coincidence events in which pileup was indicated were tagged for rejection during later analysis. Once during each beam burst a mercury-relay pulser was triggered to provide reference signals for digital gain stabilization. The pulser events were tagged and the stabilization was carried out off-line.

Pulse heights corresponding to the two energies and the time difference were digitized and recorded on computer-compatible magnetic tape by a Nuclear Data Series 160 buffer-tape multiparameter analyzer. One of the modifications made to the analyzer for these experiments was the addition of a 10-bit monitor register, each bit of which could be set independently from a front-panel connector. This register was used just like an additional 10-bit ADC. A patch panel was also added to select the 36 bits recorded for each event from the total of 50 available from the four ADC's and the monitor register. The identifying pulses associated with the four distant detectors, and the labeling pulses from the pulser and the pileup inspector, were each connected to one bit in the monitor register. The output of the monitor coincidence circuit set one bit in the monitor register and was also used to initiate processing of the monitor count. Gating logic was such that equal fractions of both monitor counts and real events were lost by analyzer dead time.

Several calibration procedures were necessary for

[22] C. W. Williams and J. A. Biggerstaff, Nucl. Instr. Methods **25**, 370 (1964).

both energy and time measurements. The energy calibrations were based on Cf^{252} fission-fragment pulse-height spectra and the mass-dependent energy calibration scheme of Schmitt *et al.*[23] Corrections for energy losses in the UF_4 target and Formvar backing were determined from measurements of the energy lost by Cf^{252} fission fragments in passing through the backing alone and through the target plus backing; the loss through the target alone was obtained by difference. To a very good approximation dE/dx for fission fragments in any particular medium is proportional to the square root of the fragment energy and nearly independent of the fragment mass.[24] The energy loss of a given uranium fission fragment was thus taken to be proportional to the square root of its energy with a proportionality constant determined from the Cf^{252} data. Corrections thus calculated for one-half the target thickness and for the backing plus one-half the target were multiplied by the appropriate trigonometric factors and applied to fragments leaving the front and back, respectively. These corrections were usually 3–4 MeV for one-half the target and 8–10 MeV for the backing plus one-half the target.

The time system required three different calibrations: one for the zero-time channel, or intercept; one for the slope of the time versus channel-number curve; and one for the slewing correction.[25] The time (slope) calibration was based on the Cf^{252} fragment velocity spectrum of Schmitt *et al.*[23] Both the time and energy calibrations were determined with a precision of $\approx 1\%$.

The data on magnetic tapes were processed event by event on either an IBM 7094 or a CDC 6600 computer. In order to save computer core space, the processing was divided into two phases. The data tape was read in the first phase, and all the events from a particular one of the four detectors were sorted into energy and time pulse-height spectra and also into energy-energy and energy-time two-parameter distributions. Events in which the inspector bit or more than one detector bit was set were rejected as they were read, although they could also be sorted into various spectra, if desired. Various criteria were applied to the pulse heights to reject events which could not have arisen from two coincident fragments. These were (a) upper and lower limits on the time pulse height to eliminate negative flight times and to keep the accepted events within the linear region of the TAC and (b) an effective lower limit on the sum of the two energy pulse heights to eliminate events in which both energies were low. (This limit was always less than a corresponding limit on the sum of the two computed energies which was applied later.) The remaining, accepted events were written event by event on a scratch tape or disk for the second phase of the processing, in which they were converted to energies and masses and sorted into various spectra and two-parameter distributions.

Inspection of the pulser events through the course of the measurements showed that, since drift in the energy systems was less than 0.3%, no stabilization was necessary for the fragment energies. The drift in the time system was sometimes as much as 1% and, because the delays were such that the zero-time pulse height was near the full-scale output of the TAC, the error introduced into the flight-time measurement by this drift was as much as $\approx 5\%$, depending on the actual flight time. The drift was found to be common to all four distant detectors and thus must have been introduced by some common element. It was established from calibrations before and after experiments that the drift was entirely in slope, or gain; the zero, or intercept, was stable. Digital gain stabilization was performed as follows. As the data tapes were read, the average pulser peak position was computed for every 200 pulser events. A gain correction factor was calculated from this average pulser peak position, and, if it was significantly different from the current correction factor, it was entered into a table of correction factors to be applied to the pertinent sets of events during the second phase of data processing. This method introduces no broadening due to statistical fluctuations. It would have introduced some broadening if a large drift had occurred during one of the 200 pulse intervals; however, such drifts were rarely observed, and the width of a gain stabilized pulser peak from a run of several days duration during which large drifts did occur was only insignificantly greater than that obtained in a 20-min calibration.

The pulse heights were converted to energies, velocity, and mass, event by event, in the second phase of the data processing. A random number, distributed between -0.5 and $+0.5$, was added to each pulse height to eliminate binning fluctuations in the various transformed spectra. The time pulse height was corrected for gain drift and time walk (slewing), and the time difference Δt was obtained by subtraction from the zero-time position. An iterative procedure was necessary to transform the pulse heights into energies, mass, and one velocity. Energies were calculated from the Schmitt mass-dependent calibration formula[23]

$$E_{i,n}=(a_i+a_i'M_{i,n-1})X_i+b_i+b_i'M_{i,n-1}, \qquad (1)$$

where the subscript i refers to the fragment in detector 1 or detector 2 (detector 1 is always the near detector and detector 2 is always the distant detector) and the remainder of the subscript refers to the pass number. The symbols a_i, a_i', b_i, and b_i' are calibration constants, X_i is the pulse height, and $M_{i,n-1}$ is the fragment mass from the previous iteration. For fragment 2 the velocity is obtained from

$$V_{2,n}=\frac{d_2}{\Delta t}\left[1-\frac{d_1}{d_2}\left(\frac{M_{1,n-1}}{M_{2,n-1}}\frac{E_{2,n}}{E_{1,n}}\right)^{1/2}\right], \qquad (2)$$

[23] H. W. Schmitt, W. E. Kiker, and C. W. Williams, Phys. Rev. **137**, B837 (1964).
[24] J. B. Cumming and V. P. Crespo, Phys. Rev. **161**, 287 (1967).
[25] Methods for making these calibrations were developed by L. P. Remsberg and F. Plasil.

where d_1 and d_2 are the distances from the target to the detectors. The term in the square brackets is a correction for the flight time to the near detector. If the momenta of the two fragments were always equal and opposite in the laboratory system, the mass ratio in the correction factor could be replaced by the more accurately known energy ratio. Fragment masses were obtained from

$$M_{2,n}=2E_{2,n}/V_{2,n}^2 \quad (3)$$

and

$$M_{1,n}=M-M_{2,n}, \quad (4)$$

where M is an estimated average total mass of the two fragments. The calculation was repeated until

$$|M_{2,n}-M_{2,n-1}|<0.1.$$

Convergence was usually achieved in 3–6 passes. Finally, the energies were corrected for losses in the target and backing with the equation[24]

$$E_i=E_{i,n}+k_i\sqrt{E_{i,n}}, \quad (5)$$

where k_i are correction factors obtained from the measured losses of Cf^{252} fission fragments passing through the target and backing. Note that the fragment masses are obtained from the energies of the already degraded fragments and are not subject to error or dispersion from the target energy-loss correction.

As mentioned above, M_1 is obtained by subtracting M_2 from an estimated total mass M. The actual total mass M_1+M_2 for any given event is, of course, not known, and thus the use of an average value M introduces an uncertainty into E_1 because of its dependence on M_1 and also into V_2 (and thus M_2) because of the presence of M_1 in the correction term in Eq. (2). An error of 10% in the estimated total mass M introduces an error of 2% in E_1 and an error of 2 amu in M_2, independent of the value of M_2. The estimated total mass M was adjusted to be twice $\langle M_2\rangle$ at each detector angle because of the symmetric nature of the detection system and the near-symmetric angles. Thus the average values of E_1 and M_2 are nearly free of error due to this effect, and the *limits* of the dispersion introduced are about 3% for E_1 and 3 amu for M_2.

Initial trial values of the masses $M_{1,0}$ and $M_{2,0}$ were taken to be equal to $\frac{1}{2}M$. The mass ratio $M_{1,0}/M_{2,0}$ in Eq. (2) was set equal to 2 for the first pass, however. Because of these inconsistent starting conditions, convergence was not tested for until after the second pass. This procedure was adopted when it was found that events with a mass ratio M_1/M_2 greater than about 2 converged slowly or not at all because in these cases the correction term in Eq. (2) is large. Starting the iteration procedure with a fairly large correction term improved the convergence rate of events with large M_1/M_2 but had very little effect on the rapid convergence of events with small mass ratios and thus small correction terms. Even so, events with a velocity ratio V_2/V_1 greater than about 3, which corresponds roughly to a mass ratio greater than 3, failed to converge. Events which gave ridiculous masses, velocities, or energies were rejected (such events arise from accidents), and events which did not meet the convergence criterion were individually listed for inspection in the computer printout.

Masses and energies for events arising from accidental coincidences were obtained from data in which the time channel number was outside the upper and lower limits of the time pulse height. Time channel numbers from these events were assigned uniformly within the upper and lower limits through the use of a random-number generator, and they were then processed in the same manner as regular events. The nonlinearity of the time-to-pulse-height converter was taken into account when the number of time channels outside the limits was chosen, so that there would be the same time for accidental coincidences in both sets of data, and so that the accidentals could be directly subtracted from the regular events. As expected, most of these accidentals were either rejected or failed the convergence test.

The performance of the entire system was checked by replacing the target with a Cf^{252} source on a thin support and accumulating at least 10^4 events with each of the four distant detectors. These data were processed in exactly the same manner as those from the UF_4 targets (except for different target-thickness corrections), and the resulting mass and energy spectra were compared with published data[23] on Cf^{252}. These checks, performed just before and/or just after each run, provided a test of the proper operation of the experimental apparatus, the data processing, and the calibration procedures, but *not* the actual calibrations, since they depend on Cf^{252}.

From an assumed energy resolution of 1 MeV and the measured time resolution of $\approx$0.45 nsec, the mass resolution was calculated to be 4 amu for the entire fission-product range of masses. This resolution is independent of fragment mass because of the varying contributions of time and energy uncertainties between low-energy slow heavy fragments and high-energy fast light fragments. The mass spectra of Cf^{252} obtained with this system were about as expected on the basis of the published mass spectrum[23] and a 4-amu resolution.

III. RESULTS

Parameter Boundary Values

Before presentation of detailed results of these experiments it is useful to analyze the effective threshold values of the parameters which were determined. There were actually two conditions which set thresholds for fission event detection: (a) an upper limit to the fragment-pair flight-time difference and (b) a data processing limit to the allowable fragment velocity ratio.

The maximum flight-time differences, 71 nsec in one set of experiments and 80 nsec in the other, correspond to minimum velocities for fragment 2 of 0.36 and 0.32

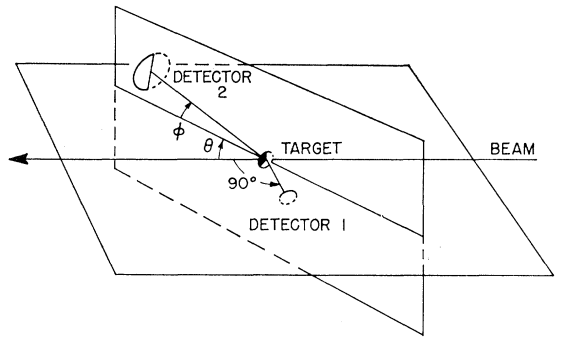

FIG. 2. Geometrical arrangement of beam, target, and detectors for fission fragments in coincidence. Detector 1 was fixed for all experiments at the 90° angle shown; detector 2 was moveable both in the in-plane angle θ and the out-of-plane angle ϕ.

cm/nsec when the velocity ratio V_2/V_1 is 3 and of 0.54 and 0.48 cm/nsec when V_2/V_1 is $\frac{1}{3}$. Light fragments are expected to have high velocities; thus the limitation should affect only the slower heavy fragments. This was indeed the case; events with velocities near the thresholds were found only for fragments with masses greater than $\approx$125. Heavy fragments with velocities between 0.5 and 0.55 cm/nsec were observed in runs with the longer time cutoff but not in runs with the shorter time cutoff. The numbers of these events ranged from $\approx$0.5 (in the units of Fig. 3) at the peak of the correlation to $\approx$0.1 in the vicinity of the 30 contour. Since the number of events per unit velocity is always decreasing with decreasing velocity in this low-velocity region, it can be concluded that the threshold in V_2 caused a negligible number of fission events to be missed.

The second threshold-setting condition was the failure of the iteration procedure for values of the velocity ratio V_2/V_1 greater than $\approx$3. This corresponds, on the average, to mass ratio M_1/M_2 of 3. It is interesting and useful to note that if the energetics of low-energy fission are assumed, the threshold in V_2 implies a minimum of $\approx$0.3, on the average, in the mass ratio M_1/M_2. Thus the two restrictions on fragment velocity produce a roughly symmetric restriction on the mass ratio:

$$\tfrac{1}{3} \lesssim M_1/M_2 \lesssim 3.$$

Angular Correlation

The angular correlation between coincident members of fission-fragment pairs was obtained from measurements of the event rate as a function of the angular positions of the distant detectors, with the near-detector proton-beam angle at the target set at 90°. The in-plane and out-of-plane angles θ and ϕ are defined in Fig. 2; the results are shown in Fig. 3. These data, obtained from several experiments during two running periods, were normalized by use of the fission monitor. The normalization was done in such a way that the numbers in Fig. 3 represent very nearly the actual numbers of net counts obtained, except in the region of the contour lines, where additional data were acquired. Accidental coincidences, averaging about 1 at all angles, have been subtracted, giving rise to some negative numbers in Fig. 3.

The most probable angle in the correlation is $\theta=89°$ and $\phi=0°$, only 1° forward of collinearity. The full widths at half-maximum (FWHM) of the over-all distributions both in-plane (summed over the out-of-plane angles) and out-of-plane (summed over the in-plane angles) are 13°. The over-all mean in-plane angle is 85.8°, or 4.2° forward of collinearity. Since the angular resolution of the system is estimated to be a roughly bell-shaped curve with a FWHM of 5°, only the detailed shape at the peak of the correlation is obscured by the resolution, if there is no fine structure elsewhere in the correlation.

Both the motion of the fissioning nucleus and recoil momenta resulting from postfission particle evaporation cause the paths of the two fission fragments to deviate from collinearity. The momentum of the fissioning nucleus is the vector sum of the momentum imparted by the fast cascade and the recoil momenta from all the prefission evaporated particles. Both the prefission and postfission evaporated particles are emitted essentially isotropically in the system of a moving nucleus, and, except for possible differences in their spectra, they have the same broadening effect per evaporated particle on the angular correlation. Broadening due to particle evaporation and cascade recoil are of similar magnitude and cannot be separated experimentally. The fairly large number of events found at angles greater than 90° can be accounted for by combined evaporation broadening and experimental angular resolution, so that these events provide no direct evidence for cascade momenta in the backwards direction.

Masses, Energies, Momenta, and Velocities

At several angles near the peak of the correlation large amounts of information were collected to obtain statis-

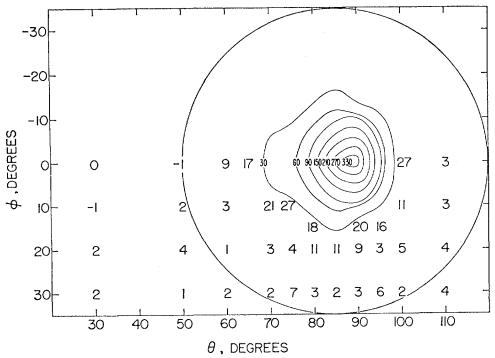

FIG. 3. Contour diagram of coincidence rate observed in the fission of uranium by 2.9-GeV protons as a function of the angles θ and ϕ subtended by detector 2 at the target. Detector 1 was always fixed, as shown in Fig. 2. Numbers are approximately the measured number of events at each angular setting.

TABLE I. Properties of fragments from fission of uranium by 2.9-GeV protons at various fragment-pair correlation angles θ and ϕ defined in Fig. 2. Listed are mean masses $\langle M_2 \rangle$, mean momenta $\langle P_2 \rangle$, and mean velocities $\langle V_2 \rangle$ for single fragments and mean total kinetic energies for fragment pairs $\langle E_T \rangle$. In parentheses, following each quantity, is the standard deviation of the distribution.

ϕ (deg) \ θ (deg)	70	80	90	100	
20		95.5(22.0)	100.7(24.1)		$\langle M_2 \rangle$
10		99.2(19.8)	110.2(20.2)		(amu)
0	100.1(23.7)	106.4(20.4)	110.5(19.7)	103.2(21.6)	
20		145.1(18.4)	142.3(18.5)		$\langle E_T \rangle$
10		149.1(17.0)	153.5(17.3)		(MeV)
0	145.2(19.5)	154.2(16.9)	162.0(15.4)	148.1(17.3)	
20		115.1(16.5)	118.0(16.8)		$\langle P_2 \rangle$
10		119.5(13.6)	128.1(14.4)		[(MeV amu)$^{1/2}$]
0	117.6(14.7)	126.6(13.8)	131.1(11.5)	121.1(15.6)	
20		1.262(0.284)	1.225(0.271)		$\langle V_2 \rangle$
10		1.249(0.252)	1.197(0.223)		[(MeV/amu)$^{1/2}$]
0	1.235(0.292)	1.228(0.228)	1.225(0.214)	1.217(0.246)	

tically significant distributions of the various parameters. The mean values and standard deviations of these distributions are given in Table I, and the distributions at two angles are plotted in Fig. 4. At all other angles the shapes of the distributions are much the same as those at $\theta=80°$, $\phi=0°$; however, the means and widths (standard deviations) do change, as shown in Table I. Statistical uncertainties of the means in Table I are all about 1% or less and those of the standard deviations of the distributions range from 1 to 5%. Over-all uncertainties in the mean values, which include the statistical uncertainties, uncertainties in the calibrations, and allowances for possible systematic effects, are estimated to be 2–3%.

The mass spectrum at $\theta=90°$, $\phi=0°$ shows a distinct contribution from asymmetric fission, not seen at any

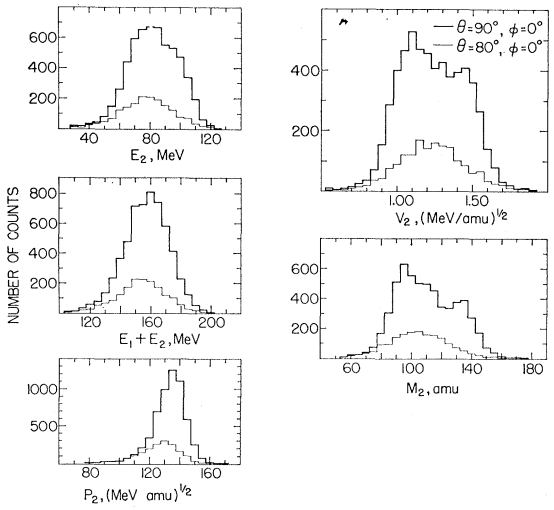

FIG. 4. Spectra of mass, velocity, momentum, and kinetic energy for single fragments from the fission of uranium by 2.9-GeV protons. Also shown is the distribution of total kinetic energy of both fragments. The upper curve in each case is for collinear events; the lower is for events at $\theta=80°$, $\phi=0°$.

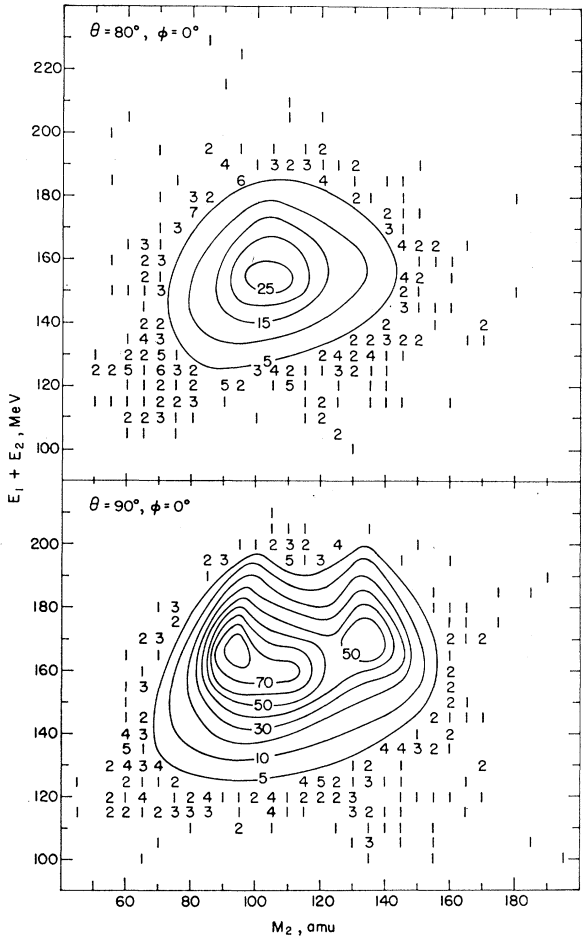

FIG. 5. Contour diagrams of coincidence event rate in fission of uranium by 2.9-GeV protons as a function of the two variables: $E_T=E_1+E_2$, the sum of the kinetic energies of the two fragments, and M_2, the mass of a single fragment. The upper plot was obtained at the detector angles $\theta=80°$, $\phi=0°$; the lower plot is for $\theta=90°$, $\phi=0°$.

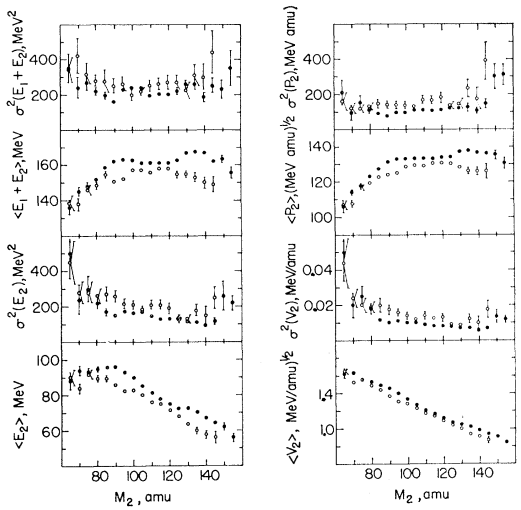

FIG. 6. Fragment properties observed in the fission of uranium by 2.9-GeV protons as a function of mass of one fragment. For single fragments the individual plots show mean values of velocity, momentum, and energy. Also shown is the dependence of mean total kinetic energy on mass of one fragment. In each case variances are given. Closed circles are data for detector angles $\theta=90°$, $\phi=0°$; open circles are for angles $\theta=80°$, $\phi=0°$.

of the other angles. Asymmetric fission in heavy nuclides is predominant only at relatively low excitation energies, and fission fragments from low-excitation-energy events are nearly collinear because low excitation energy is associated with low momentum transfer in the cascade as well as in a relatively small evaporation sequence.

In Fig. 5 there are shown for two θ, ϕ angles the number of fission events as a function of two parameters: total fragment kinetic energy and mass of one fragment. The interesting and unusual shape of the $\theta=90°$, $\phi=0°$ distribution undoubtedly results from fissions representing a broad range of excitation energies. The lower energies lead to predominantly asymmetric fission with total kinetic energy averaging $\approx$170 MeV and fragment masses centered at $\approx$135 and $\approx$95; higher excitation energies lead predominantly to symmetric fission centered on the average at mass $\approx$105 amu and total energy of 155–160 MeV. Properties of this higher-excitation-energy component of the fission may be seen relatively isolated in the 80°, 0° contours. Inspection of the 90°, 0° contours shows that mass distributions at constant E_1+E_2 have pronounced double-humped shapes for all total energies above $\approx$170 MeV. No such structure at high total energies is observed in the $M-E_T$ contour plots at any of the other angles.

Means and variances of the distributions of E_2, E_1+E_2, V_2, and P_2 for 5-amu bins in M_2 are shown in Fig. 6 for the same two angles. Again, the data at all the other angles resemble those at $\theta=80°$, $\phi=0°$ except for shifts to lower values of M_2, E_2, etc., as indicated in Table I. The contribution from asymmetric fission at $\theta=90°$, $\phi=0°$ is clearly evident in each of the four distributions as maxima or at least inflection points at masses of $\approx$95 and $\approx$135. That the mean total energies and momenta are not reflection-symmetric about some mean mass can be explained qualitatively with the quite reasonable assumption that there is a distribution in total mass of fission-fragment pairs. There should be a weak correlation between the mass of a fragment and the mass of both fragments, i.e., light fragments tend to be associated with a low average total mass and heavy fragments with a higher total average mass. The lack of reflection symmetry in plots of mean total energies and momenta follows directly from the positive correlation between the over-all mean total energy or momentum and the mean mass, as shown in the data of Table I. Except for the effects of the distribution in the total mass, the data in Figs. 5 and 6 are very much like similar data from fission in bombardments at much lower energies.[15,16] [26]

It is interesting to compare data from this work with the 90° momentum spectra of the nuclides Mo^{99}, Pd^{103}, Ba^{131}, and Ba^{140} produced in the irradiation of uranium by 2.2-GeV protons. These spectra, measured by Crespo *et al.*[10] with a radiochemical differential range technique, in effect represent integrals over the entire angular correlation with all partner fragments and include as well any contributions from nonfission processes. They are shown in Fig. 7 along with two momentum spectra at each mass from this work, one representing events near collinearity and one representing events which are quite noncollinear. For the latter curves, data from three angles with about the same degree of noncollinearity and the same mean momenta ($\theta=90°$, $\phi=20°$; $\theta=80°$, $\phi=10°$; and $\theta=70°$, $\phi=0°$) were combined in order to have a sufficient number of events to define the shapes of the spectra reasonably well. Each mass was taken as a bin 5 units wide, centered at 99, 103, 131, or 140. All of the curves were normalized to the same area.

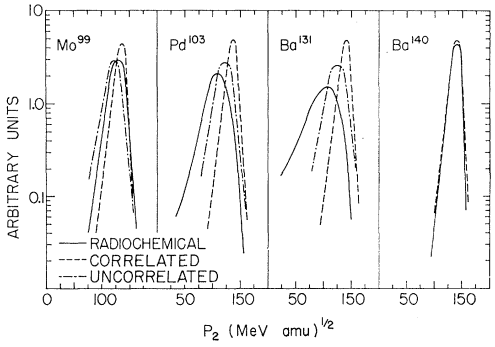

FIG. 7. Fragment momentum spectra observed from uranium irradiated with protons. Solid lines represent the radiochemical data of Crespo *et al.* (Ref. 10) obtained with 2.2-GeV protons for the nuclides indicated. Other sets of lines are fission data of these experiments, in each case a mass group 5 amu wide, at the appropriate mass value. Dashed curves are for collinear events, $\theta=90°$, $\phi=0°$; dot-dashed curves represent a composite of noncollinear events. All of the curves are normalized to the same area.

[26] See, for example, J. P. Unik and J. R. Huizenga, Phys. Rev. **134**, B90 (1964); several references to other results are given in Ref. 16.

The Mo^{99} spectrum is closely matched by the counter data. This is the most favorable case for comparison since Mo^{99}, as a cumulative yield on the neutron-excess side of stability, represents $\approx 70\%$ of the total yield at $A=99$. The spectrum for Pd^{103} is centered at a lower momentum than the counter data; however, the cumulative yield of the neutron-deficient nuclide Pd^{103} is only $\approx 10\%$ of the total cross section at $A=103$, and thus the Pd^{103} spectrum is not inconsistent with the low-momentum tails of the counter spectra. In the heavy-mass region, the spectrum for Ba^{140}, which represents $\approx \frac{1}{3}$ of the yield at mass 140, matches the spectrum for collinear events very well; this suggests that Ba^{140} is primarily associated with asymmetric fission. The Ba^{131} spectrum differs from the counter spectra in both the shape and position of the peak; the yield of the neutron-deficient nuclide Ba^{131} represents $\approx \frac{1}{3}$ of the total yield at $A=131$, and although an accurate normalization of these spectra is not feasible, an approximate normalization makes it clear that the low-momentum components are not found in the counter spectra.

IV. DISCUSSION

Angular-Correlation Distribution and Low-Momentum Events

It is of importance to consider what types of fission or fissionlike events may not have been detected in these experiments. Though one detector was always at an angle of 90° to the beam direction, it was concluded earlier that the observations were made with a nearly unbiased sample of all fissions producing fragments of any plausible masses. There are observed (Fig. 3) a few events far from the peak in the angular correlation. The number of these was sufficient to determine only that they satisfied the experimental threshold requirements. In order to estimate the fraction of all events sufficiently correlated to be well characterized, the volume under the surface contained within the circle in Fig. 3 was obtained by integration using a form of Simpson's rule. Approximately one-third of the total volume was found under the surface from the peak to the 150 contour, approximately one-third under the surface between the 30 and 150 contours, and the remaining one-third under the surface between the 30 contour and the circle. The average counting rate at the circle is about 2 in the units of Fig. 3 and about 1 for those data points at some distance from the circle. If the counting rate over the entire hemisphere outside the circle is taken to be 1 and the integration is carried out over the entire hemisphere, the volume increase amounts to 17% of that inside the circle. However, the counting rate would be expected to continue to decrease below the level of 1, particularly in the backwards direction; and the fraction of all events found within the circle is therefore probably somewhat greater than the lower limit of 1/1.17 or 86%.

Experimental data from 15 angles outside or near the circle in Fig. 3 were combined in an attempt to obtain improved statistics on these events. Almost one-half of the total were accidental events, and the best that can be said about the rest is that they do not appear to be anomalous. A particularly careful search was made for evidence of events with low kinetic energy, $100>E_1+E_2>50$ MeV. No such evidence was found.

Failure of these experiments to detect all of the low-momentum components of Ba^{131} found in the radiochemical recoil experiments cannot be attributed entirely to experimental thresholds. The momentum cutoff, as determined by the lower limit of the velocity, is 70 $(\text{MeV amu})^{1/2}$ and is rather sharp, and the momentum spectrum for Ba^{131} decreases relatively slowly in this region. One is thus led to the conclusion that at least some of the low-momentum Ba^{131} fragments have no partner fragments detectable in this experiment; indeed, Crespo *et al.*[10] did estimate that 18% of the Ba^{131} is produced by a nonfission process. This conclusion, however, does not rule out the possibility that low-momentum nuclei in this mass region could be produced through some breakup mechanism characterized by mass ratios exceeding 3 or by fragment-pair velocities quite substantially smaller than those associated with low-energy fission. It needs to be emphasized, the foregoing notwithstanding, that the fragment velocity thresholds given earlier did indeed permit the detection, had they been produced with partners of reasonable mass, of fragments having momenta considerably smaller than anything actually observed. For example, at mass ≈ 130, as may be seen in Fig. 7, the event rate drops very rapidly at momenta below the most probable, and there is no evidence that any substantial fraction of events is associated with fragments having momenta in the vicinity of the threshold, about 70 $(\text{MeV amu})^{1/2}$, equivalent to an energy of 38 MeV.

Correlation Angle and Fission-Mass Division

An obvious feature of the data, remarked upon previously, is the significant contribution of asymmetric fission to the events at $\theta=90°$, $\phi=0°$. The mass spectrum of collinear events can be resolved into two components: one, contributing about $\frac{2}{3}$, in the form of a symmetric peak like that at $\theta=80°$, $\phi=0°$, and the remainder from a double-peaked distribution such as would be expected from asymmetric fission. Predominantly asymmetric mass division is characteristic of the fission of heavy nuclides ($A \gtrsim 225$) at low excitation energies, whereas symmetric mass division predominates in the fission of lighter fissile nuclides and also in the fission of heavy nuclides at higher excitation. The excitation energy above which symmetric fission predominates depends on both Z and A, but for nuclei near stability it ranges from ≈ 20 MeV for $Z=89$ to ≈ 50 MeV for $Z=93$.[27,28] Thus,

[27] H. C. Britt, H. E. Wegner, and J. C. Gursky, Phys. Rev. **129**, 2239 (1963).
[28] E. Konecny and H. W. Schmitt, Phys. Rev. **172**, 1213 (1968).

at least $\frac{1}{3}$ of the events with $\theta=90°$, $\phi=0°$ result from cascades imparting less than $\approx$50 MeV of excitation to the residual nucleus. Further, the absence of any indication of asymmetric fission at other angles indicates that nearly all fission events which follow cascades of low deposition energy are essentially collinear. An upper limit of 10% may be estimated for the contribution of asymmetric fission to all fission events. This does not relate directly to the cascade deposition energy spectrum, however, since symmetric fission competes with asymmetric fission even at deposition energies below 50 MeV. In addition, as the work of Pate and Poskanzer[29] indicates, spallation competes especially effectively with fission when the cascade deposition energies are low, at least for deposition energies up to $\approx$200 MeV.

Cascade Deposition Energy

Average cascade deposition energies can be estimated from the mean fragment masses in Table I. Since both members of fragment pairs are always detected at or not very far from 90° to the incident beam direction, the mean total mass of fragment pairs at a given angle is twice the mean mass of the coincident fragments detected in one detector. This mean total mass varies from 221 at collinearity to 191 at $\theta=80°$, $\phi=20°$, and the difference between the target mass and the mean total fragment mass can be related to the cascade deposition energy. For 1.8-GeV protons on U^{238}, the Monte Carlo calculations of Metropolis *et al.*[30] yield an average cascade deposition energy of 50 MeV per cascade nucleon emitted, and evaporation calculations[31] indicate that, for highly excited heavy nuclei, the energy is dissipated at the rate of about 12 MeV per nucleon lost. Thus for each nucleon lost in a cascade about four nucleons are subsequently evaporated; this gives the result that the average cascade deposition energy corresponds approximately to 10 MeV per nucleon emitted. Deposition energies, derived in this manner from the difference between the target and fragment-pair masses, should be reduced by about 30 MeV; this reduction is the nuclear binding energy released as fragment excitation in the fission act, which results in the loss of about three nucleons. Average cascade deposition energies thus obtained range from 140 ± 40 MeV at collinearity to 440 ± 80 MeV at $\theta=80°$, $\phi=20°$; the error estimates are comprised of contributions from the cascade and evaporation calculations and from the mass measurements. Such an analysis is insensitive to the choice of point in the evaporation chain at which the excited nucleus undergoes fission because the excitation energy is dissipated in evaporated particles from excited fission fragments at very nearly the same rate as from excited heavy nuclei.

It is interesting to note that, although the contribution to collinear events from asymmetric fission indicates that at least $\frac{1}{3}$ of the collinear events have deposition energies less than 50 MeV, the average deposition energy for these events turns out to be 140 MeV. That the deposition energy spectrum even at this correlation angle is very broad and extends to quite high energies is not surprising; although the relation between cascade momentum transfer and deposition energy tends to restrict low-deposition-energy fission events to angles near collinearity, high-deposition-energy cascades are followed by a large evaporation sequence, which broadens considerably the correlation angle distribution. This broadening is of such magnitude that numbers of events having large cascade deposition energies and forward cascade momenta can appear at collinearity and even backwards. Moreover, the correlation found in the Monte Carlo calculations between momentum transfer and deposition energy is not strong, and some high deposition energies are associated with low momentum transfer.[32]

The over-all average mass of fission fragments, estimated by weighting the average masses in Table I with the angular correlation shown in Fig. 3, is 101 amu, with an uncertainty of 3–4 amu. This corresponds to an average number of nucleons removed from the target of 36 and thus an average excitation energy of 330 ± 70 MeV. A second estimate of the average excitation energy for all fission events can be obtained from the average value of $p_{||}/p_{\text{inc}}$, the fraction of the incident proton momentum transferred in the cascade which appears as momentum component of the excited nucleus parallel to the beam direction. This quantity can be derived from the mean value of θ because the evaporated particles only broaden the angular correlation and do not much affect fragment velocities. Thus, one may write

$$\cos\langle\theta\rangle\approx\langle v_{2||}/V_2\rangle,$$

where $v_{2||}$ is the laboratory velocity component parallel to the beam direction of the fragment in detector 2 and the other quantities have been defined. For the fragment in detector 1 at 90° to the beam, $v_{1||}=0$; consequently,

$$\langle v_{||}\rangle\approx\tfrac{1}{2}\langle v_{2||}/V_2\rangle\langle V_2\rangle\approx\tfrac{1}{2}\cos\langle\theta\rangle\langle V_2\rangle. \quad (6)$$

Here $\langle v_{||}\rangle$ is the average velocity component along the beam direction of the cascade products which eventually yield fission fragments. As may be seen in Table I and in Fig. 8, $\langle V_2\rangle$ varies only little with θ, and with the values $\langle V_2\rangle=1.23$ (MeV/amu)$^{1/2}$ and $\langle\theta\rangle=85.8°$, $\langle v_{||}\rangle$ becomes 0.044 (MeV/amu)$^{1/2}$. If one uses a value of 230 amu for the average mass of the residual nuclei after the cascade, $\langle p_{||}\rangle$ becomes 10.1 (MeV amu)$^{1/2}$ and the ratio $\langle p_{||}\rangle/p_{\text{inc}}$ is equal to 0.084. The relationship $E^*/E_{\max}=0.75\langle p_{||}\rangle/p_{\text{inc}}$, obtained from Monte Carlo cascade calculations, has often been used to calculate

[29] B. D. Pate and A. M. Poskanzer, Phys. Rev. **123**, 647 (1961).
[30] N. Metropolis, R. Bivins, M. Storm, J. M. Miller, G. Friedlander, and A. Turkevich, Phys. Rev. **110**, 204 (1958).
[31] I. Dostrovsky, P. Rabinowitz, and R. Bivins, Phys. Rev. **111**, 1659 (1958).
[32] N. T. Porile, Phys. Rev. **120**, 572 (1960).

E^* values from various radiochemical recoil data[3]; with this equation and the value 0.084 one obtains an excitation energy average of 240±40 MeV, to be compared with the value 330±70 MeV calculated by the different method mentioned earlier.

Analysis of Mean Velocities of Fragments

The mean total energies and mean fragment momenta in Table I decrease from their maximum values at collinearity in direct proportion to the mean fragment masses. In other, more striking words, the mean fragment velocity is nearly the same at all angles.

Mean fragment velocity is a very useful parameter for characterizing high-energy fission because it is not changed appreciably either by particle evaporation or, for fragments emitted at or near 90° to the beam direction, by the cascade momentum transfer. It has already been mentioned that velocity components contributed to fission fragments by particle evaporation, either before or after fission, have the effect of increasing the width of the fragment velocity distribution, but very nearly cancel in the mean velocity; the same is true for perpendicular components of cascade-imparted velocities. The velocity given to the fragments by $p_{||}$ does not cancel, but, since most fragments are detected not very far from 90°, the increase in the resultant mean velocity will be of the order of 1%.

Close examination of the data in Table I does indicate

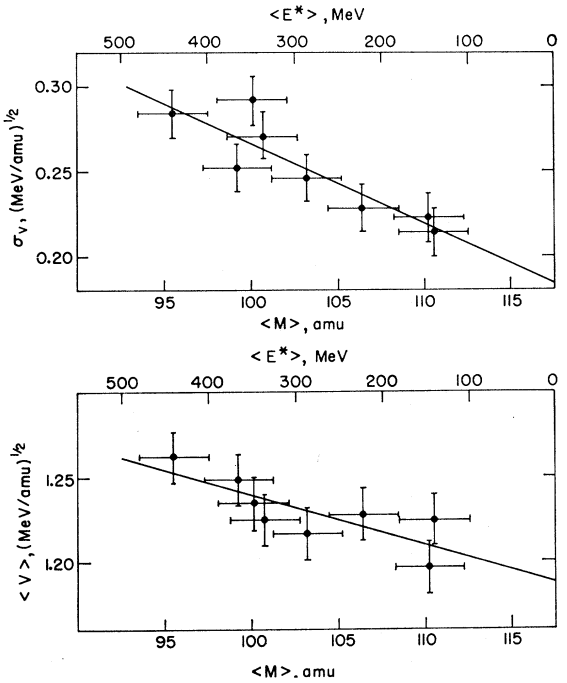

FIG. 8. Mean velocity of fragments from fission of uranium by 2.9-GeV protons as a function of average fragment mass observed in all fissions occurring at a given correlation angle. Relation between mean cascade deposition energy $\langle E^* \rangle$ and $\langle M \rangle$ is given in the text. The upper part of the figure shows the standard deviations in the velocity distributions. Each point in the figure represents all data taken at one individual correlation angle.

that some correlation exists between mean fragment velocity, as measured at the several angles, and mean fragment mass. These mean velocities are plotted as a function of their corresponding mean masses in Fig. 8; the straight line was obtained by least-squares fitting. If mean fragment masses are related to mean cascade deposition energies, as described above, the straight line in Fig. 8 can be transformed directly into the expression

$$\langle V \rangle = 1.19 + (1.5 \pm 0.5) \times 10^{-4} \langle E^* \rangle, \qquad (7)$$

where $\langle V \rangle$ is in the units $(\text{MeV/amu})^{1/2}$ and $\langle E^* \rangle$ is the mean cascade deposition energy in MeV. The slope, which amounts to a 1% increase in mean velocity for 80-MeV increase in mean excitation energy, can at least partially be accounted for by the increase in both the number of evaporated particles and $\langle p_{||} \rangle$ with increasing excitation energy. The standard deviations of the velocity distributions, also plotted in Fig. 8, increase with decreasing mean fragment mass or increasing mean excitation energy. This broadening of the velocity distributions is expected from increasing widths of the mass distributions as well as from increasing numbers of evaporated particles.

Fragment velocities determined in these experiments may be compared with average fragment velocities measured in fission of various nuclei at lower excitation energies. Average fragment velocities in the thermal-neutron fission of U^{233}, U^{235}, and Pu^{239} are 1.21, 1.21, and 1.22 $(\text{MeV/amu})^{1/2}$, respectively.[33] The 13-MeV proton fission of Ra^{226} yields a well-known triple-peaked mass distribution, and the average fragment velocities of the asymmetric and symmetric components were found to be 1.24 and 1.18 $(\text{MeV/amu})^{1/2}$, respectively.[28] Fission of Bi^{209} induced by 53-MeV α particles has been investigated by Plasil *et al.*[34]; only symmetric fission was observed, with a mean fragment velocity of 1.18 $(\text{MeV/amu})^{1/2}$. It appears that asymmetric fission is characterized by a mean fragment velocity of $\approx$1.22 $(\text{MeV/amu})^{1/2}$ and symmetric fission by a mean velocity of $\approx$1.18 $(\text{MeV/amu})^{1/2}$.

In Eq. (7), the constant term 1.19 $(\text{MeV/amu})^{1/2}$ may be interpreted as the mean fragment velocity in the moving system of the fissioning nucleus; within experimental uncertainty it is identical with the value 1.18 $(\text{MeV/amu})^{1/2}$ for the average fragment velocity in low-energy symmetric fission. This supports strongly the notion that the fission process in high-energy proton reactions is essentially the same as that which occurs with low-energy projectiles.

Comparison of Experimental Results with Liquid-Drop-Model Predictions

The dynamic liquid-drop theory of Nix and Swiatecki[35] reproduces the gross features of low-energy symmetric

[33] J. C. D. Milton and J. S. Fraser, Can. J. Phys. **40**, 1626 (1962).

[34] F. Plasil, R. L. Ferguson, and H. L. Schmitt (private communication).

[35] J. R. Nix and W. J. Swiatecki, Nucl. Phys. **71**, 1 (1965).

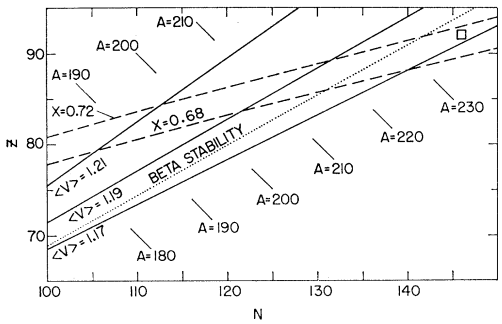

FIG. 9. Z,N plot showing loci of nuclei having equal values of mean fission-fragment velocity, as calculated on the basis of the Nix-Swiatecki liquid-drop model (Ref. 35). Loci (solid lines) are shown for three indicated values of the velocity. Lines (dashed) of constant fissility parameter x (defined in text) and the line (dotted) of β stability are also given.

fission very well. Certain approximations employed in the calculations should restrict the application of the theory to values less than 0.68 for the fissility parameter $x=(Z_f^2/A_f)/50.13$.[36] Nevertheless, Crespo *et al.*[10] have used the Nix-Swiatecki theory to reproduce average center-of-mass velocities of various fission products from the 450-MeV proton fission[37] of U^{238}, in which case the value of x for the average fissioning species is 0.72. According to the Nix-Swiatecki theory, there is very little dependence of average fragment velocity on the Z and A of the fissioning species for reasonable Z/A ratios. This is illustrated in Fig. 9, in which there are drawn several lines, each representing the Z, N function for the set of fissioning species that has a constant mean fragment velocity; for the calculation of these lines, the Nix-Swiatecki theory in the anharmonic approximation was employed.[38] The lines, essentially parallel to the line of β stability, show that there is a very small increase in mean fragment velocity with increasing neutron deficiency. Such an increase may account, at least in part, for the increase in mean fragment velocity with increasing cascade deposition energy, because the average neutron deficiency of the fissioning species is expected to increase with increasing cascade deposition energy. Nix-Swiatecki theory predicts the mean fragment velocity to be essentially independent of the excitation energy of the fissioning nuclide.

It is interesting to note that the variation, calculated from liquid-drop theory, of mean fragment velocity with Z and A of the fissioning nucleus is smaller than that calculated from what may be described as a "constant deformation model." The total fragment kinetic energy in such a model is given by

$$E_T \propto Z_1Z_2/(A_1^{1/3}+A_2^{1/3}), \tag{8}$$

which is a statement that the total kinetic energy is directly proportional to the Coulomb energy of two charged spheres in contact. Equation (8) gives the mean fragment velocity relationship[39]

$$\langle V\rangle \simeq Z_f/2A_f^{2/3}. \tag{9}$$

Variations of $\langle V\rangle$ with Z_f and A_f, i.e., $\partial\langle V\rangle/\partial Z_f$ and $\partial\langle V\rangle/\partial A_f$, from Eq. (9) are about twice as large as corresponding values from the Nix-Swiatecki liquid-drop calculations. This implies that the average separation distance between fragment charge centers for liquid-drop shapes at the scission point increases with decreasing N/Z ratio at a given A.

Hogan and Sugarman[40] have interpreted the results of their thick-target, thick-catcher recoil measurements of heavy fragments ($A\approx140$) produced in the 440-MeV proton fission of uranium as indicating that the effective charge-center separation distance at scission increases with increasing excitation energy of the fissioning nucleus. The mean fragment velocity is inversely proportional to the square root of the separation distance; thus, the $\approx10\%$ increase in separation distance deduced by Hogan and Sugarman for an excitation energy of ≈250 MeV should correspond to a decrease of $\approx5\%$ in mean fragment velocity, relative to that in low-excitation-energy fission. In a sense, this is opposite to the result of these experiments, which show that the mean fragment velocity increases with increasing mean excitation energy. There may be no contradiction between the two results, however. In the 2.9-GeV proton fission of uranium, average cascade deposition energies are high, and the fission is nearly all of the symmetric variety. In only one point of Fig. 8 is there an appreciable contribution from asymmetric fission, so that the constant 1.18 of Eq. (7) should apply. Deposition energies associated with 440-MeV proton-induced fission of uranium are much lower; there should be a substantial contribution from asymmetric fission at low excitation energies, while the higher excitation energies produce only symmetric fission. The decrease in mean fragment velocity ascribed by Hogan and Sugarman to increase in separation distance with excitation is about the same as the difference between the mean fragment velocities of asymmetric and symmetric fission given by the two values for the constant of Eq. (7).

From all the considerations above, one overriding conclusion emerges: Fission of uranium induced by

[36] The constant 50.13 in this expression for the fissility parameter is the old value used by Nix and Swiatecki (Ref. 35).

[37] N. Sugarman, H. Münzel, J. A. Panontin, K. Wielgoz, M. V. Ramaniah, G. Lange, and E. Lopez-Menchero, Phys. Rev. **143**, 952 (1966).

[38] An improved version of the dynamic liquid-drop calculation has recently become available: J. R. Nix, University of California Lawrence Radiation Laboratory Report No. 17958 (unpublished). Its application is not expected to alter significantly the conclusions to be drawn from Fig. 9.

[39] J. Terrell, Phys. Rev. **113**, 527 (1959).

[40] J. J. Hogan and N. Sugarman, Phys. Rev. **182**, 1210 (1969).

2.9-GeV protons appears to proceed by mechanisms indistinguishable from those operative at much lower bombarding energies. Any other essentially two-body breakup mechanism which can operate to produce fragments in the mass region studied in these experiments must produce fragment pairs having large mass ratios or very low velocities or both; and, moreover, such mechanisms cannot merge in a continuous way with fission.

ACKNOWLEDGMENTS

The authors take pleasure in thanking Fred Specht for his help in design of the scattering chamber used in this work. They are indebted to Joseph Lypecky, John Hennessy, and Robert Stafford for assistance in setting up working arrangements at the Cosmotron and also to J. Wooderson Glenn, III, and the Cosmotron operating staff.

PHYSICAL REVIEW VOLUME 187, NUMBER 4 20 NOVEMBER 1969

Elastic and Inelastic Proton Scattering from ^{110}Pd†

R. L. ROBINSON, J. L. C. FORD, JR., P. H. STELSON, T. TAMURA,* AND C. Y. WONG‡
Oak Ridge National Laboratory, Oak Ridge, Tennessee 37830

(Received 8 July 1969)

The differential cross sections for elastically and inelastically scattered 13.0-MeV protons from ^{110}Pd have been measured for 26 groups to levels below ~3 MeV. Optical-model parameters were obtained from a fit of the elastic data. A comparison of the predictions given by the distorted-wave theory with the experimental results for the strongly excited 2^+ level at 0.374 MeV and 3^- level at 2.038 MeV yielded values of 0.241 for β_2 and 0.134 for β_3, where β_λ is the deformation parameter of multipolarity λ. The coupled-channel theory was used to calculate cross sections for the two-quadrupole, the one-octupole–one-quadrupole, and the 6^+ three-quadrupole phonon states. It was only possible to explain the strong diffraction pattern for the cross section of the second 2^+ state by admixing the one- and two-quadrupole phonon states. Coupled-channel predictions suggest tentative spin parities of 1^-, 3^- or 5^-, 3^-, and 3^- for states at 2.135, 2.193, 2.446, and 2.778 MeV, respectively. For the 6^+ three-quadrupole phonon state, the calculated cross sections are similar to those for proton groups exciting the 1.713- and 1.933-MeV states.

I. INTRODUCTION

BECAUSE inelastic scattering by direct nuclear interaction preferentially excites collective states, it has been used extensively to investigate the quadrupole and octupole deformations of many nuclei through excitation of the collective 2^+ and 3^- states. The scattering to these states has been interpreted principally in terms of the first-order, distorted-wave (DW) theory.[1] However, because it is first-order, it is restricted to analysis of states which can be reached by a one-step process. One theoretical approach that goes beyond the DW treatment, but that is still in terms of a macroscopic description of the nucleus, is the coupled-channel theory. This has been treated in considerable detail by Tamura.[2] He has developed an extensive computer program that can calculate the differential cross sections for inelastic scattering from up to six states simultaneously. With this program, one can predict the differential cross sections for exciting higher members of rotational bands and states due to more than one-phonon vibrations of the nucleus. We have experimentally addressed ourselves to inelastic scattering studies of medium-weight nuclei whose results can be compared to calculations made by this coupled-channel program. Our purpose has been to examine to what degree some of the higher states can be explained in terms of the phonon model. Earlier we published results of the inelastic scattering of 13-MeV protons from ^{106,108}Pd,[3] ^{107}Ag,[4] and ^{112,114}Cd.[5] The present paper deals with ^{110}Pd.

The differential cross sections for 26 proton groups exciting states below ~3 MeV in ^{110}Pd are reported. The very strong groups exciting the first 2^+ and 3^- states are fitted by both the DW and coupled-channel theories. The coupled-channel theory was also used to predict the cross sections for the two-quadrupole phonon states and one-octupole–one-quadrupole pho-

† Research sponsored by the U. S. Atomic Energy Commission under contract with Union Carbide Corporation.

* Present address: University of Texas, Austin, Tex.
‡ On leave to the Niels Bohr Institute, Copenhagen, Denmark.

[1] W. Tobocman, *Theory of Direct Nuclear Reactions* (Oxford University Press, New York, 1961); R. H. Bassel, G. R. Satchler, R. M. Drisko, and E. Rost, Phys. Rev. **128**, 2693 (1962); N. Austern, *Selected Topics in Nuclear Theory* (International Atomic Energy Agency, Vienna, 1963); N. Austern and J. S. Blair, Ann. Phys. (N. Y.) **33**, 15 (1965); F. G. Perey, in *Nuclear Spin-Parity Assignments*, edited by N. B. Gove and R. L. Robinson (Academic Press Inc., New York, 1966).

[2] T. Tamura, Rev. Mod. Phys. **37**, 679 (1965); Oak Ridge National Laboratory Report No. ORNL-4152, 1967 (unpublished).

[3] R. L. Robinson, J. L. C. Ford, Jr., P. H. Stelson, and G. R. Satchler, Phys. Rev. **146**, 816 (1966).

[4] J. L. C. Ford, Jr., C. Y. Wong, T. Tamura, R. L. Robinson, and P. H. Stelson, Phys. Rev. **158**, 1194 (1967).

[5] P. H. Stelson, J. L. C. Ford, Jr., R. L. Robinson, C. Y. Wong, and T. Tamura, Nucl. Phys. **A119**, 14 (1968).